2013 European Control Conference (ECC)
July 17-19, 2013, Zürich, Switzerland.

Motion Control for Magnetic Micro-scale Manipulation

Andrew G. Alleyne, Simone Schurle, Alessandro Meo, Bradley J. Nelson

***Abstract*—This work demonstrates performance improvement in motion control under a particular set of machine system constraints. A high performance industrial magnetic micro-manipulation system, the Minimag, is introduced and modeled with both first principles and system identification. The form of the closed loop controller is constrained by operational bounds and the system software, resulting in limits to achievable performance. A model-based motion control enhancement is developed and implemented using tools from Iterative Learning Control. The resulting performance improvements indicate the benefits of motion control even when the closed loop controller is fixed. Experimental results at two different size scales (500 μm and 4.5μm) are given.**

I. INTRODUCTION AND SYSTEM OVERVIEW

The use and impact of microscale machines have grown tremendously in the past 20 years [1,2]. With increased utilization of microscale machines, across diverse fields [3], comes the demand for increasingly stringent manipulation at commensurate length scales. Automation is a key enabler for this microscale manipulation and there are emergent applications in fields such as robotic microassembly [2] and also cell mechanics [4]. Throughout the various fields of use for microscale machines, significant opportunities exist for control tools to contribute in their development and performance [3]. This article focuses on one such specific example.

Several different techniques have been proposed that can servo microscale objects to localized targets; these include both tethered actuators [5] and untethered systems. Untethered actuation can be based on dielectrophoretic [6], magnetic [7], fluidic [8], acoustic [9] or optically induced forces [10]. Depending on the application, one approach might be advantageous over the other. Magnetic forces are favorable especially in several biological applications that require a biocompatible, non-contact approach. In many of these biological applications, magnetic fields are used to manipulate small spherical objects; these objects are available in range of sizes and are functionalized as the task requires. The key to the object manipulation is the ability to precisely (<1μm) transport these systems over distances of a few to hundreds of micrometers. A magnetic manipulation system that is specifically designed for such a task is the MiniMag [11,12]. The system consists of 8 electromagnets arranged in a single hemisphere and can be incorporated into either an upright or inverted microscope (see Fig. 1.a). Magnetic samples are placed in a custom-made sample holder on the x-y-stage with the lens is located underneath.

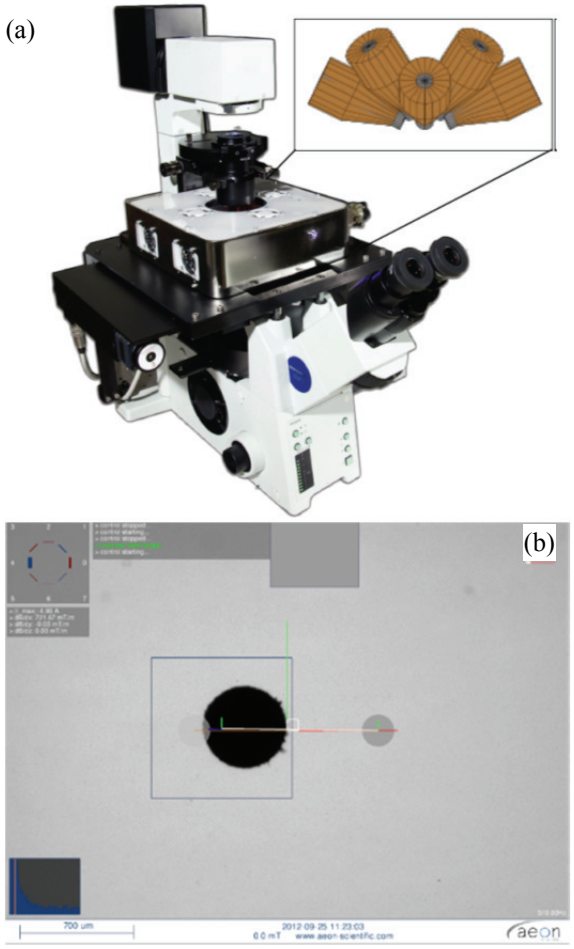

Figure 1: (a) Picture of microscope mounted MiniMag and schematic of an inverted coil configuration; (b) screenshot of the control panel Graphical User Interface (GUI).

Based on visual feedback the magnetic object can be servoed to a target location in open or closed-loop fashion. A typical scenario is depicted in Fig. 1.b. The position of the object, a 500 μm large magnetic sphere, is detected based on a visual servoing algorithm. The region of interest is indicated by the blue box. Desired trajectories that specify the task can then be loaded as system input or entered by the user through the GUI. Here, two trajectory waypoints (grey) are given as the input target signal. The interested reader is referred to [11,12, 13], and the references therein, for further details on the MiniMag system construction, use, and applications.

A. Alleyne is with the Univiersity of Illinois, Urbana-Champaign, 1206 West Green Street, Urbana, IL, 61801 (phone: +1-217-244-9993; e-mail: alleyne@illinois.edu)

S. Schurle and B. Nelson are with ETH Zurich. (email: schuesim@ethz.ch and bradley.nelson@iris.mavt.ethz.ch)).

A. Meo is with the University of Pisa, Italy (email: alessandro.meo@gmail.com)

The primary control challenge is the generation of point to point motions as depicted in Fig 1.b. The goal is to minimize settling time to reach a new target position. This would be a typical minimum time bang-bang optimal control problem except for some key constraints. For the purpose of this discussion, the MiniMag is a closed software system; the software constrains the form of controllers implementable. Secondly, hard constraints on the input current magnitudes provide input saturation. Finally, the disturbances encountered may be uncertain since the environments (e.g. cell substrates) are not known a priori. To achieve the goal of minimum settling time, while respecting current machine/environment constraints, this work leverages motion control tools to augment the existing baseline controller in a feedforward fashion.

The rest of this paper is organized as follows. Section II outlines the basic system model and discusses control-relevant constraints. Section 3 outlines a motion control approach that improves performance while observing the structural system constraints. Section 4 illustrates experimental results. A conclusion summarizes the main results and discusses future hardware, software, and control improvements.

II. SYSTEM MODELING AND CONSTRAINTS

The following is an abbreviated overview of the MiniMag magnetic manipulation system. We present the magnetic force generation on a sphere and simplify it to decoupled 2nd order systems. The interested reader is referred to [11,12], and the references therein, for complete details.

A. Modeling and Identification

Here we have an object (sphere) and 8 electromagnets that can superpose their fields to create motion on the object. The force (N), that accelerates a magnetic object exposed to an externally applied magnetic field **H** with a flux density $\mathbf{B}=\mu_0\mathbf{H}$ (with $\mu_0 = 4\pi\times10^{-7}$Tm/A for the permeability of vacuum), is described by:

$$\mathbf{F} = \nu\left(\mathbf{M}\cdot\nabla\right)\mathbf{B} \tag{1}$$

where **M** is the volume magnetization in [A/m] of the object of a certain volume *v*. Since there is no electric current flowing through the region occupied by the body, Maxwell's equations require that $\nabla\times\mathbf{B}=0$ and, after rearranging (1), the force can be expressed as:

$$\mathbf{F} = \nu\begin{bmatrix}\frac{\partial B}{\partial x} & \frac{\partial B}{\partial y} & \frac{\partial B}{\partial z}\end{bmatrix}^T\mathbf{M} \tag{2}$$

For our system that operates the object in a suspended fluid, the resulting velocity of the object is determined by the fluidic force $\boldsymbol{F}_{drag}$ that opposes the applied magnetic force.

$$\mathbf{F}_{ext} + \mathbf{F}_{drag} = m\ddot{x}. \tag{3}$$

In order to induce the desired motion on an object located at a point **P** to be moved to a certain target destination, the required magnetic force, hence the required magnetic field and gradients, needs to be determined. The magnetic field magnitude is usually fixed by the user and chosen such as that a sufficient magnetic moment is achieved. The system controller of the MiniMag is based on setting a target flux density, orientation, and unit force as

$$\begin{bmatrix}\mathbf{B}\\ \mathbf{F}_{unit}\end{bmatrix} = \mathcal{A}\left(\hat{\mathbf{M}},\mathbf{P}\right)\mathbf{I} \tag{4}$$

where $\mathcal{A}\left(\hat{\mathbf{M}},\mathbf{P}\right)\mathbf{I}$ is a 6x8 matrix that relates the 8 input currents, $\mathbf{I}=[i_1 \ldots i_8]^T$, to the generated field and gradient or force vectors respectively along the x, y and z directions. The magnetization vector **M** is normalized in order to remove its dependency on the object's size and material properties and is written as $\hat{\mathbf{M}}$. Details on the system modeling can be found in [11,12,13].

After suitable transformations, given in (4), the system can be decoupled along its axes and represented as a simple inertia within a viscous environment that is subject to external forcing.

$$\begin{aligned} m\ddot{x} + b\dot{x} &= F_x + F_{x\_dist}\\ m\ddot{y} + b\dot{y} &= F_y + F_{y\_dist}\\ m\ddot{z} + b\dot{z} &= F_z - mg \end{aligned} \tag{5}$$

The system in (5) assumes an accurate decoupling transformation in (4) as well as a spherical object for manipulation. This has been verified in [11,12,13]. One difference between (3) and (5) is the gravitational offset in the z-axis. Additionally, F_{x_dist} and F_{y_dist} are the effects of the surface forces interacting with the object. For objects interacting with biological surfaces, these friction/adhesion forces can be complex and are unknown to the controller.

Considering the x-axis motion as an exemplar, and ignoring F_{x_dist} for now, the transfer function between input force and output position can be represented as a type 1 second order system

$$\frac{X(s)}{F_x(s)} = \frac{1}{ms^2+bs} \tag{6}$$

The actual force on the particles can be represented as a field gradient in the direction of motion. Therefore, equation (6) can be rewritten as (7) where we assume the coil inductance and current dynamics are sufficiently fast as to be ignored.

$$\frac{X(s)}{U_x(s)} = \frac{X(s)}{\partial B_x/\partial X} = \frac{k_x}{ms^2+bs}\cdot\frac{m}{T/m} \tag{7}$$

As indicated in Section 1, the feedback measurement is provided by a camera/microscope visual feedback system which operates at 15 Hz for the results in this paper. Utilizing a bilinear Tustin transformation [16]

$$s \approx \frac{2}{T}\bullet\frac{1-z^{-1}}{1+z^{-1}} \tag{8}$$

the system can be written in discrete time as

$$\frac{X(z^{-1})}{U_x(z^{-1})} = \frac{k_x\left(1-2z^{-1}+z^{-2}\right)}{\left(\frac{4m}{T^2}+b\right)-\frac{8m}{T^2}z^{-1}+\left(\frac{4m}{T^2}-b\right)z^{-2}} \tag{9}$$

where z^{-1} is the Z transform of the shift operator. As shown in (9), the basic structure is a 2nd order numerator and denominator system.

The basic model form for the system can be used as a guide in grey-box system identification [17] by constraining

the form of the models. Since it is a type 1 system, closed loop identification was utilized with a simple P-controller providing feedback to a square wave reference. Figure 2 and 3 show the identification results for two different object sizes: 500 microns and 4.5 microns, respectively. These spheres moved in a silicon oil medium supported on a glass substrate. Matlab's system identification toolbox was used with a model constraint of 2nd order numerator and denominator polynomials so as to fit the grey-box structure. Additionally a single step delay was added to accommodate the sampled data framework. The oscillations in the step responses are partially due to the gain P resulting in underdamped closed loop performance. Only the x-axis results are shown with the other axes performing similarly.

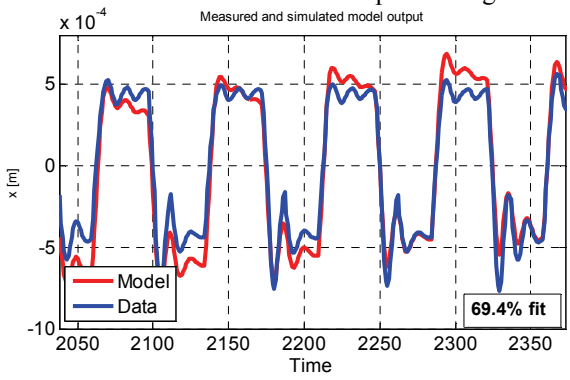

Figure 2. System ID results for 500 μm particle

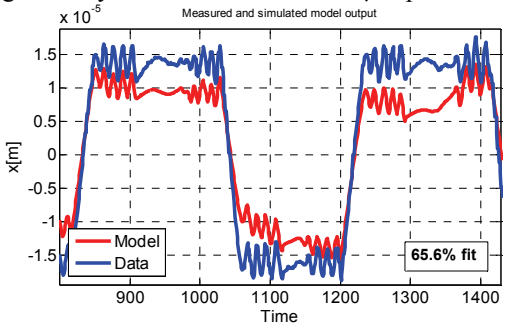

Figure 3. System ID results for 4.5 μm particle

The identified models for both sizes are given below.

$$\left.\frac{X(z^{-1})}{\partial B_x/\partial X}\right|_{500\,\mu m} = 10^{-6} \times \frac{-2.465z^{-1}+133.1z^{-2}}{1-1.238z^{-1}+0.2342z^{-2}}\frac{m}{T/m} \quad (10)$$

$$\left.\frac{X(z^{-1})}{\partial B_x/\partial X}\right|_{4.5\,\mu m} = 10^{-8} \times \frac{-9.574z^{-1}+33.28z^{-2}}{1-1.149z^{-1}+0.1491z^{-2}}\frac{m}{T/m} \quad (11)$$

The large difference in gain associated with the two sizes results from the significant variation in magnetic material contained in the two volumes. Compare with the larger particle, the smaller one takes more than two orders of magnitude greater gradient to induce similar motion.

B. System Constraints

The basic second order system models in (6) work well for sufficiently small signals. To generate the necessary fields requires significant current in each of the coils. This becomes more relevant with smaller particles since higher field gradients are required to generate motion-inducing forces. There are 2 types of saturations present in the MiniMag systems and they are illustrated in Figure 4. First, due to the soft-magnetic core of these electromagnets, there exists saturation in the magnetic field as a function of applied current to the electromagnets. This is typically referred to as a BH curve or hysteresis curve and is an inherent property of the magnetic material used. Secondly, in order to manage heat buildup during extended periods of use, a hard limit should be placed on the maximum gradient to manage heat buildup and allow for extended periods of use. From a controller perspective, the combination of these two saturations results in an input saturation on the amplifiers affecting each electro-magnetic coil in the system.

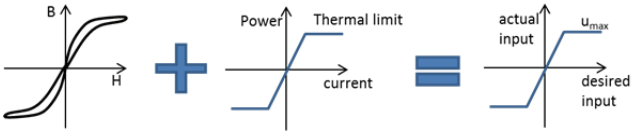

Figure 4. System saturation constraints

A second, and equally important constraint, is the closed nature of the controller software structure. The commercial software is produced by Aeon Inc. [16] and is a Linux-based C++ environment. Since it is designed for end users such as biological, medical, and pharmaceutical professionals it has a predefined Proportional-Integral-Derivative (PID) controller structure that is not amenable to reconfiguration. The only modifications that can be made to the feedback controller are the gains. Additionally, reference signals are given as step changes in desired position between 2 points in the workspace. The format of references cannot be changed and the reference signals themselves are input by the user as graphical waypoints on an Aeon GUI and hence are not accessible to the controller. This constraint is similar to closed architecture machine tool controllers [19].

The challenge for the motion control design is how to affect higher performance motion control under these constraints: saturation and closed software architecture.

III. MOTION CONTROL DESIGN

A. Motion Control Overview

In general, motion control consists of several parts: (i) a feedback controller, which is fixed in this case; (ii) sensor elements, which are limited to 15 Hz here; (iii) a reference generator, which is constrained to step commands for this system and inaccessible to the controller; and (iv) a feedforward element. The use of feedforward and feedback is termed 2 Degree of Freedom (DOF) control. Given the system constraints, the primary degree of freedom available for design and manipulation is the feedforwad controller which can be added as a plug-in to the existing controller framework.

B. Closed Loop Iterative Learning Control

Iterative Learning Control (ILC) [20] has proven itself to be a valuable tool for generating feedforward trajectories using learned behavior. This requires a series of iterations on the machine to learn the appropriate feedforward input trajectories. The goal is to improve motion control

performance in a simple, yet high performance, feedforward framework. To do so, we will utilize ILC design to create implementable feedforward signals.

ILC utilizes a system representation of the form

$$y_j(k) = P(q)u_j(k) + d(k) \tag{12}$$

where k is the time index, j is the iteration index, q is the forward time-shift operator $qx(k) \equiv x(k+1)$, y_j is the output, u_j is the control input, and d is an exogenous signal that repeats each iteration. Standard assumptions include:

- $P(q)$ is a stable plant.
- Exogenous signals repeat each iteration; reference = $r(k)$ and disturbances = $d(k)$.
- The initial condition $y(0)$ is identical each iteration.

The basic ILC structure under consideration in this work is a frequency domain representation given by (13).

$$u_{j+1}(k) = Q(q)\left(u_j(k) + L(q)e_j(k)\right) \tag{13}$$

Here, $e_j(k) = r(k) - y_j(k)$ is the error, which is accessible, $L(q)$ is the learning update operator and $Q(q)$ is the so-called Q-filter to provide robustness. Both learning update and Q-filter are linear operators given in the discrete domain.

If the plant model is well known, then ILC plant inversion techniques can be utilized to achieve deadbeat convergence [20]. Essentially, setting $Q(q) = 1$ and $L(q) = P^{-1}(q)$ results in the learning update law

$$u_{j+1}(k) = u_j(k) + P^{-1}(q)e_j(k) \tag{14}$$

Since we consider the MiniMag controller to be a closed system, with no access to the operator specified reference generation, the parallel ILC plug-in architecture is necessary. Figure 5 shows a parallel ILC framework that would utilize frequency domain technique for design of learning filters L, Q.

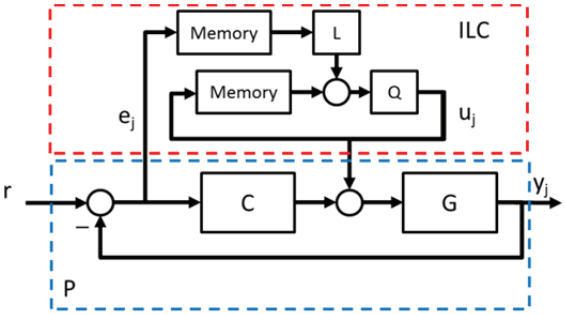

Figure 5. Parallel plug-in ILC configuration [20]

For the parallel arrangement of Figure 5, the system dynamics can be rewritten as in Equation (15) to match the standard ILC format of (12).

$$\begin{aligned} y_j(k) &= \underbrace{(1+G(q)C(q))^{-1}G(q)}_{P(q)} \cdot u_j(k) \\ &+ \underbrace{(1+G(q)C(q))^{-1}G(q)C(q)r}_{d(k)} \end{aligned} \tag{15}$$

Therefore, the plant to be inverted involves the closed loop system. If the ILC in (14) can be applied with the $P(q)$ from (15) then, in the absence of modeling error, the ILC would converge in exactly one iteration.

The benefit of including the ILC, as opposed to simple plant inversion feedforward approaches, is the ability to incorporate the effects of the un-modeled F_{x_dist} and F_{y_dist} in the feedforward signal. Since we do not have models for them, we allow their effects to propagate through $P^{-1}e_j(k)$ and map to the feedforward input.

C. Motion Control Design

The design approach utilizes the fixed PID structure of the Aeon controller and augments it with the feedforward signal resulting from a closed loop $P^{-1}(q)$ type of ILC. Since the system is already type 1, there is no need for an integrator to handle steady state errors for step reference trajectories that are input by the end user. A simple P-controller is sufficient. Note the open loop plants of (10) and (11) are non-minimum phase. Therefore, the P-control gain should be sufficiently low as to maintain stability. Figure 6 shows the root locus of the 4.5 µm bead under P-control with the chosen gains: $C(q) = K_p = 3.0 \times 10^5$. A similar root locus exists for the 500 µm bead.

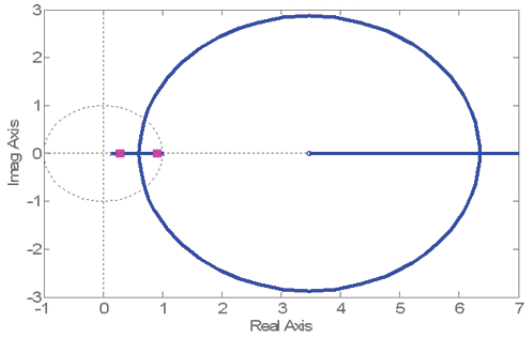

Figure 6. Root Locus for 4.5 micron system under P-control

Still using the 4.5 µm bead as the example

$$\begin{aligned} G_{4.5\mu m}(z) &= 10^{-8} \times \frac{-9.574z^{-1} + 33.28z^{-2}}{1 - 1.149z^{-1} + 0.1491z^{-2}} \\ C_{4.5\mu m}(z) &= 3.0 \times 10^5 \end{aligned} \tag{16}$$

where z is the Z-transform of the discrete time shift index q. Therefore,

$$\begin{aligned} P_{4.5\mu m}(z) &= \frac{G_{4.5\mu m}(z)}{1 + G_{4.5\mu m}(z)C_{4.5\mu m}(z)} \\ &= 10^{-8} \frac{-9.574z^{-1} + 33.28z^{-2}}{1 - 1.178z^{-1} + 0.249z^{-2}} \end{aligned} \tag{17}$$

For the 500 mm bead the results are identical in structure but with different coefficients.

$$\begin{aligned} G_{500\mu m}(z) &= 10^{-6} \times \frac{-2.465z^{-1} + 133.1z^{-2}}{1 - 1.1238z^{-1} + 0.2342z^{-2}} \\ C_{500\mu m}(z) &= 1.0 \times 10^3 \end{aligned} \tag{18}$$

Therefore,

$$\begin{aligned} P_{500\mu m}(z) &= \frac{G_{500\mu m}(z)}{1 + G_{500\mu m}(z)C_{500\mu m}(z)} \\ &= 10^{-6} \times \frac{-2.465z^{-1} + 133.1z^{-2}}{1 - 1.124z^{-1} + 0.367z^{-2}} \end{aligned} \tag{19}$$

The closed loop plants in (17) and (19) are both causal. Moreover, the zero of $P(q)$ is outside the unit circle in both cases; i.e. non-minimum phase. This is due to the fact that the feedback will not change the zero locations. Therefore,

inverting $P(q)$ to use in (14) results in an unstable non-causal system which clearly cannot be implemented.

There are multiple methods available for approximating the inverse of non-minimum phase systems to use in (14) including the Zero Phase Error Tracking Controller (ZPETC) [21] and the Zero Magnitude Error Tracking Controller [22]. Given a plant $P(z)$ with unstable zeros $B_u(z)$

$$P(z) = \frac{B(z)}{A(z)} = \frac{\overbrace{B_s(z)}^{\text{stable zeros}}\overbrace{B_u(z)}^{\text{unstable zeros}}}{A(z)} \tag{20}$$

the ZPETC approximation for the plant inversion is given as

$$P^{-1}(z) \approx \frac{A(z)z^{-N}}{B_s(z)B_u^*(z)} \tag{21}$$

with

$$B_u^*(z) = \frac{\left(B_u(1)\right)^2}{B_u^f(z)} \tag{22}$$

Here $B_u^f(z)$ is the so-called 'flipped' version of the unstable polynomial obtained by reversing the order of the polynomial coefficients [22]. The term z^{-N} in (21) contains additional shifts to ensure causality of the inverse. This is equivalent to adding N high frequency poles as a filter in order to make the overall system causal. In this work, the filter is designed to be low pass with a break frequency well below the z^N filter having N poles at the origin. In this case, a first order low pass filter $B_{lpf}(z)$ is sufficient.

$$P^{-1}(z) \approx \frac{A(z)}{B_s(z)B_u^*(z)} \cdot \frac{1}{B_{lpf}(z)} \tag{23}$$

As will be seen in Section III.D, the design of $B_{lpf}(z)$ is very important to the overall 2 DOF ILC-based performance.

Since the ILC design is a single iteration plant inversion approach, the feedforward term obtained from (14) is the pseudo-inverse operating on the error signal. Figure 7 shows a step reference command, output motion, and an error signal for the 500 micron bead. Similar responses exist for the 4.5 micron bead system. Using the inversion technique without the low pass filter $B_{lpf}(z)$ in (23) results in a pseudo differentiation of the error signal given in Figure 7. This poses 2 problems; the impulsive function resulting from the differentiation of Figure 7 provides a delta function with a magnitude above the saturation threshold. Secondly, the duration of the impulse is short relative to the sample time, possibly leading to imprecise application of the impulse.

D. *Feedforward signal generation*

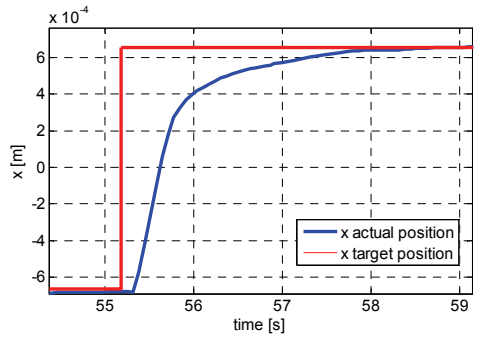

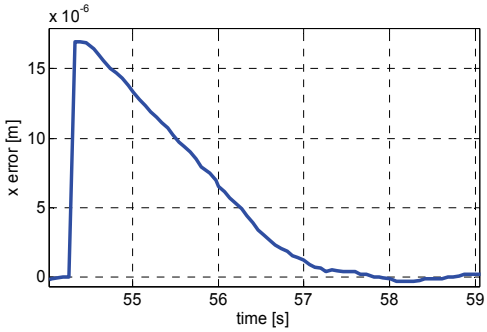

Fig 7. 500 μm particle closed loop control. Top: target step reference and position output response, Bottom: error

With a first order filter time constant chosen to be 0.1 seconds, and a sample rate of 15 Hz, $B_{lpf}(z)$ can be written as follows:

$$B_{lpf}(z) = \frac{1}{4}\frac{(1+z^{-1})}{(1-.5z^{-1})} \tag{24}$$

In addition, the resulting feedforward signal u_{ff} is subject to the saturation limits given in Section II.B.

$$\begin{aligned} u_{ff} &= sat\left(P^{-1}(z)\cdot e(k)\right) \\ &\approx sat\left(\frac{A(z)}{B_s(z)B_u^*(z)B_{lpf}(z)}\right) \end{aligned} \tag{25}$$

Here the *sat* function is defined as:

$$sat(x) = \begin{cases} 1 & \forall \;\; x > 1 \\ x & \forall \;\; |x| \le 1 \\ -1 & \forall \;\; x < -1 \end{cases} \tag{26}$$

The resulting feedforward signal is given in Figure 8. The results for the 4.5 micron system are similar. However, the saturation limit is increased from 1 T/m to 4 T/m in order to effect any movement in the particles. This increased limit results in an increase to the operating temperature of the power electronics and care must be taken to manage this for extended system usage.

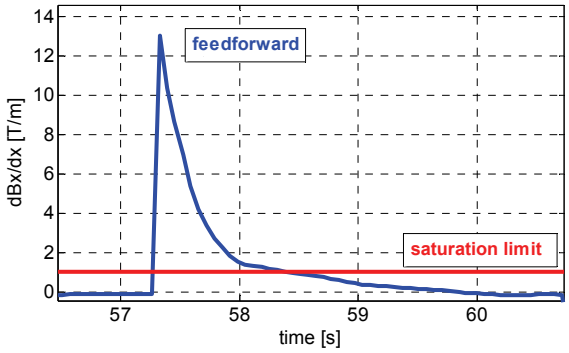

Figure 8. Feedforward signal generated from the error signal in Figure 7.

Upon examination, the feedforward compensation can be reasonably approximated with an exponential that is clipped by the saturation limit. Fortunately, this type of a signal structure is easily incorporated into the current MiniMag Aeon controller framework without altering the closed PID

structure of the controller. A C++ routine can utilize the error magnitude at the initial step and use it to scale a clipped exponential impulse response.

IV. COMPARISON RESULTS

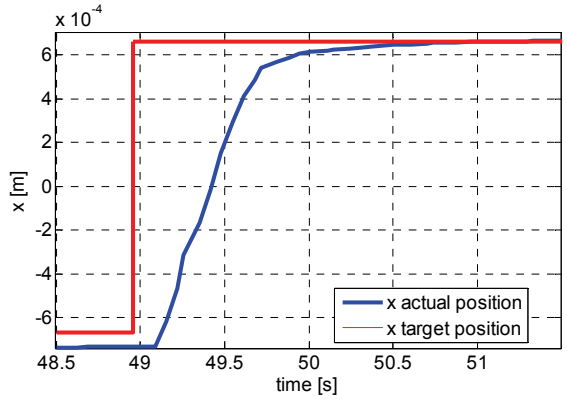

Fig 9. 500 µm particle closed loop control with feedforward

The results of the system with and without the feedforward compensation can be seen by comparing Figure 7 with Figure 9. The time taken to get within 10 % of steady state is reduced from 2.05 sec to 0.96 sec. This ~50% reduction in motion time, with similar motion profiles, directly translates into a higher bandwidth machine that is more responsive to user commands. Similar comparisons can be made for the 4.5 micron bead. However, in this case the saturation has a more significant effect.

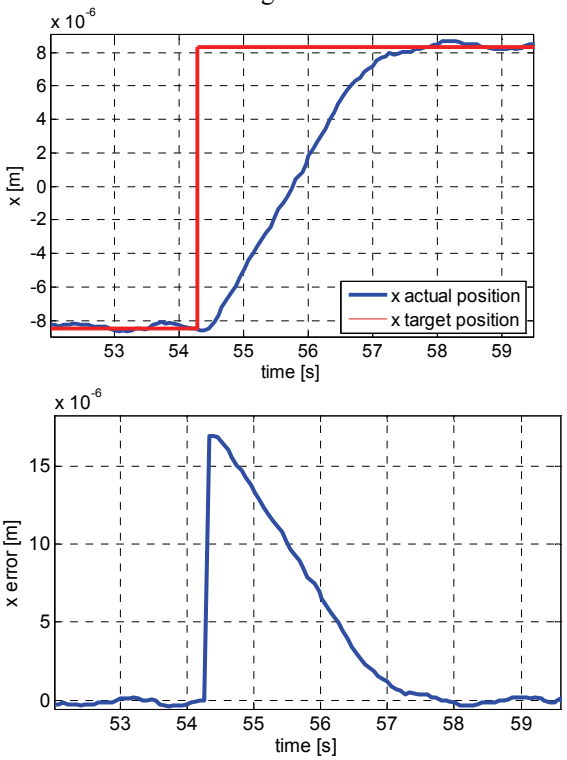

Figure 10. 4.5 µm particle closed loop control. Top: target step reference and position output response, Bottom: error.

Figure 11 shows the step response of the system under feedback control for the 4.5 micron bead. Figure 10 shows the similar step response when the feedforward approach is implemented. The improvement is significantly less than with the larger bead; the response time dropped from approximately 3.3 seconds in the feedback case to 3.2 seconds in the feedback + feedforward case.

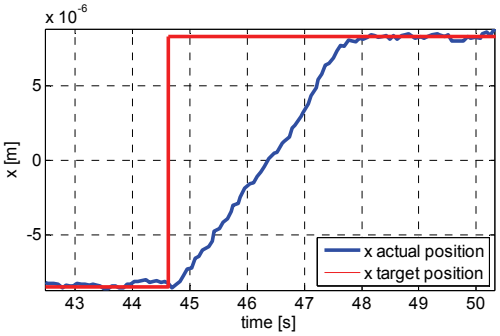

Fig 11. 4.5 µm particle closed loop control with feedforward

The primary reason can be seen in Figure 12 which demonstrates the saturation effect on the overall 2 DOF control input. The system input is saturated for nearly the entire duration of the step response indicating that little else could be done to improve the controlled bandwidth.

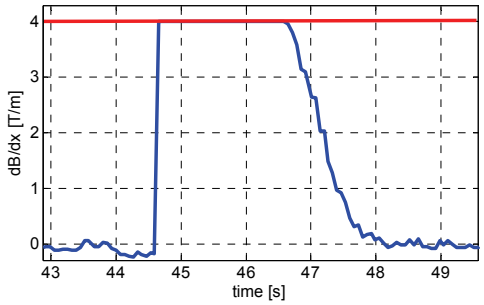

Figure 12. Saturated input signal, including feedback and feedforward terms for the 4.5 µm particle.

V. CONCLUSIONS

The paper presents a device-specific control solution. The MiniMag system is a unique magnetic manipulation device offering non-contact motion control of magnetized particles. Due to the particular nature of the system, and its targeted end users, there are two system constraints: saturation and a closed software environment. This article demonstrated that a feasible augmentation is able to improve the overall system's motion control performance for a range of particle sizes. An inverse based ILC was implemented with a ZPETC approximation for the plant inverse. This gained up to 50% improvement for the 500 µm particle used here. The performance improvement is significantly greater for larger particles due to increased magnetization strength.

Other solutions exist for improving system performance and an examination of Figure 6 indicates the feedback controller was not designed aggressively. A higher gain feedback controller, possibly with the utilization of a PD or lead compensation framework, could improve tracking performance to within the limits of saturation. However, as shown below in Figure 13, this leads to a very noisy control signal; something that results in unwanted buildup of the

systems thermal loads. The 2 DOF ILC-based approach, illustrated for comparison in Figure 14, provides good motion control without severely taxing the system's power electronics capabilities.

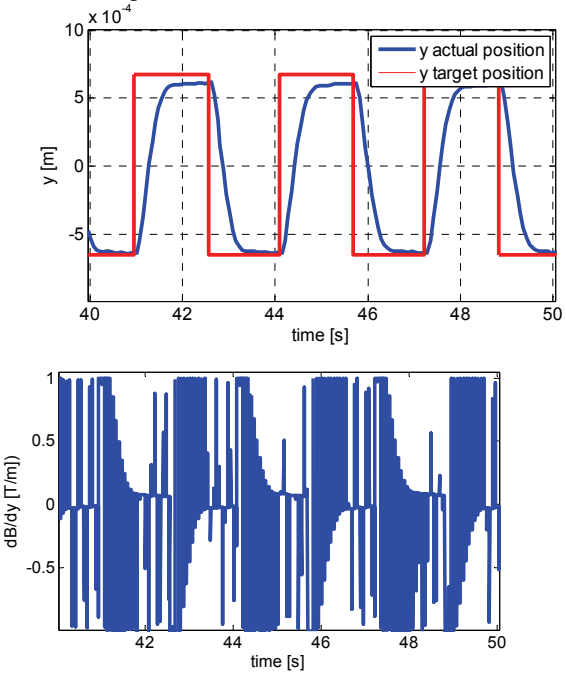

Figure 13: Output tracking (top) and input signal (bottom) for a high gain PD controller on the Y-axis of the 500 µm particle

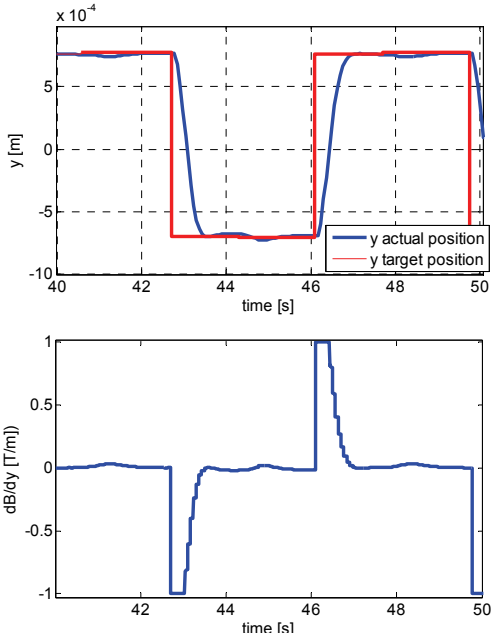

Figure 14: Output tracking (top) and input signal (bottom) for a P-control with feedforward controller on the Y-axis of the 500 µm particle

The motion control enhancements given here would be suitable for other magnetic manipulation types of systems. Possible future work, specific to the MiniMag, involves the improvement of power electronics so as to mitigate the effect of saturations. Additionally, the conversion to an open software architecture also warrants investigation. Other potential work involves the investigation of large F_{x_dist} and F_{y_dist} in environments other than silicon oil on glass. In this work they were small because of the benign medium. The configuration of the feedforward input obtained by the ILC, shown in Fig 7 and 8, would likely be shifted should the object be in contact with a tissue substrate or some other that had complex adhesion mechanics.

REFERENCES

[1] K. Peterson and W. McCulley, "Micromachines on the March," *IEEE Spectrum*, vol. 31 (5):20-31, 1994.

[2] M. Gauthier and S. Régnier, Robotic microassembly, John Wiley and Sons, 2010.

[3] B. Shapiro, "Workshop on Control of Micro- and Nano-Scale Systems", in *IEEE Control Systems Magazine*, vol 25: 82-88, 2005.

[4] Jaydev P. Desai, Anand Pillarisetti, and Ari D. Brooks, "Engineering approaches to biomanipulation, " in *Annu. Rev. Biomed. Eng*, 9:35–53, 2007.

[5] N. Dechev, W. L. Cleghorn and J. K. Mills, "Microassembly of 3-D microstructures using a compliant, passive microgripper", *Journal of Microelectromechanical Systems*, vol. 13 (2): 176-189, 2004.

[6] E. M. Freer, O. Grachev, X. Duan, S. Martin and D. P. Stumbo, "High-yield self-limiting single-nanowire assembly with dielectrophoresis" *Nature Nanotechnology*, vol. 5, 625-625 , 2010.

[7] K. C Neumann and A. Nagy, "Single-molecule force spectroscopy: optical tweezers, magnetic tweezers and atomic force microscopy," *Nature Methods*, vol. 5(6):491, 2008

[8] R. Probst, Z. Cummins, C. Ropp, E. Waks, and B. Shapiro, "Flow control of small objects on chip," *IEEE Control Systems Magazine*, vol. 32 (2): 26–53, 2012.

[9] M. Hagiwara, T. Kawahara, Y. Yamanishi, T. Masuda, L. Feng, and F. Arai, "On-chip magnetically actuated robot with ultrasonic vibration for single cell manipulations," *Lab on a Chip*, vol. 11, pp. 2049–2054, 2011.

[10] R. Won, "Optical trapping: Microassembly, " *Nature Photonics*, vol. 3: 317, 2009.

[11] S. Schuerle, S. Erni, M. Flink, B.E. Kratochvil, and B. J. Nelson, "Three-Dimensional Magnetic Manipulation of Micro- and Nanostructures for Applcations in Life Sciences," *IEEE Transactions on Magnetics*, vol. 49, no 1, pp. 321-330, 2013

[12] S. Schuerle, K. E. Peyer, B. E. Kratochvil, and B. J. Nelson. "Holonomic 5-DOF magnetic control of 1D nanostructures,", in *Proc. of the International Conference on Robotics and Automation*, 2012.

[13] M. Kummer, J. J. Abbott, B. E. Kratochvil, R. Borer, A. Sengul, and B. J. Nelson. "OctoMag: An electromagnetic system for 5-DOF Wireless micromanipulation," *IEEE Transactions on Robotics*, vol. 26:1006–1017, 2010.

[14] Franklin, G., Powell, J.D., Emami-Naeini, A, Feedback Control of Dynamic Systems, Prentice Hall, 2002

[15] Soderstrom, T., and Stoica, P., System Identification, Englewood Cliffs: Prentice Hall, 1989.

[16] http://www.aeon-scientific.com/

[17] Pritschow, G., Altinas, Y., Jovane, F., Koren, Y., Mitsuishi, M., Takata, S., van Brussel, H., Weck, M., Yamasaki, K., "Open Controller Architecture-Past, Present, Future," *CIRP Annals-Manufacturing Technology*, Vol. 50, No., 2, pp. 463-470, 2001.

[18] Bristow,D. A., Tharayil,M. , and Alleyne, A. G., "A Survey of Iterative Learning Control," *IEEE Contro System Magazine*, vol. 26, no. 3, pp. 96-114, June 2006.

[19] Tomizuka, M., "Zero Phase Error Tracking Algorithm for Digital Control," *ASME Journal of Dynamic Systems, Measurement and Control*, Vol. 109, pp. 65-68, 1987

[20] Butterworth, J., Pao, L., Abramovitch, D., "The Effect of Nonminimum-Phase Zero Locations on the Performance of Feedforward Model-Inverse Control Techniques in Discrete-Time Systems," *Proc. of the 2008 American Control Conference*, pp. 2696-2702.